ASTRONOMY & ASTROPHYSICS
SUPPLEMENT SERIES

Astron. Astrophys. Suppl. Ser. **133**, 299–316 (1998)

Long-term spectroscopy of η Carinae[⋆,⋆⋆]

I. The high and low excitation phases

A. Damineli[1,⋆⋆⋆], O. Stahl, A. Kaufer, B. Wolf[2], G. Quast[3], and D.F. Lopes[4]

[1] JILA University of Colorado and National Inst. for Standards and Technology, Boulder, CO 80309-0440, U.S.A.
[2] Landessternwarte, Königstuhl, D-69117 Heidelberg, Germany
[3] Observatório Nacional, R. General José Cristino 77, 20921-440 Rio de Janeiro, Brazil
[4] Laboratório Nacional de Astrofísica/CNPq, R. Estados Unidos 154, Caixa Postal 21, 37500-000 Itajubá, Brazil

Received April 20; accepted June 12, 1998

Abstract. Quantitative measurements of line parameters in the spectrum of η Carinae are presented for both the broad and narrow line components. A total of 655 spectral features were measured in the spectral range 3850 Å to 11000 Å, giving a comprehensive view of the behavior of atomic transitions ranging from a few to tens of electron volts. The spectrum on the phase of maximum intensity in the high excitation lines (1995) is compared with that on minimum intensity (June 1992), showing that at this phase the high excitation lines disappear but the broad components of low excitation lines strengthens. We reject a number of previous line identifications and propose several new ones, including Fe II, [Fe II], [Fe III], [N II], and the near-infrared Ca II triplet. Some lines commonly used to diagnose density, temperature, chemical composition, and reddening were found to be blended, urging a revision of the results based on previous data. The existence of double-peaked lines, suggested in previous papers, is ruled out. In the case of hydrogen lines, the apparent double-peaks are shown to be real absorption components. The velocity field in the inner 2″ around the central star shows additional components previously unknown. The phases of high and low excitation in η Carinae are discussed in light of a recently proposed binary system. We suggest a temperature $T \sim 16000$ K for the primary star, what indicates that it is close to the beginning of the core helium-burning evolutionary stage.

Key words: stars: emission-line, Be — stars: Hertzsprung–Russel (HR) diagram — stars: individual: η Carinae — binaries: general

1. Introduction

Eta Carinae (η Car) is one of the most interesting stellar objects known. It is disconcerting that after 150 years of research, the real nature of the central star remains unknown. A review of the many problems involved can be found in Davidson & Humphreys (1997). The recent discovery of a 5.52 year periodicity (Damineli 1996) opened a new road to explore this object. Moreover, its spectrum seems to be understandable in light of the binary nature proposed by Damineli et al. (1997, hereafther DCL); also see Davidson (1997).

Since Le Sueur reported the first visual observation in 1870, η Car has been the subject of many publications. During the last century, its spectrum has been characterized by strong H I, Fe II, and [Fe II] lines (Cannon 1916; Hoffleit 1933; Whitney 1952; Thackeray 1953; Walborn & Liller 1977). For brief time intervals in 1948, 1965, 1981, 1987, and 1992, the spectrum has shown remarkable fading of the high excitation lines, such as [Ne III] and [Fe III] (Gaviola 1953; Rodgers & Searle 1967; Thackeray 1967; Whitelock et al. 1983; Ruiz et al. 1984; Zanella et al. 1984; Allen et al. 1985; Bandiera et al. 1989; Altamore et al. 1994; Damineli 1995; Damineli 1996). Such behavior led to the idea of a *normal* spectrum that occasionally is replaced by an *event* spectrum during shell episodes (Zanella et al. 1984). Long term monitoring carried out since 1989 at Laboratório Nacional de Astrofísica (LNA/CNPq – Brazil) and 1992 at European Southern Observatory (ESO – Chile) has shown that the spectrum varies continuously

Send offprint requests to: damineli@iagusp.usp.br

⋆ Based on data collected at European Southern Observatory and Laboratório Nacional de Astrofísica.

⋆⋆ Table 1 is only available in electronic form at the CDS via anonymous ftp to cdsarc.u-strasbg.fr (130.79.128.5) or via http://cdsweb.u-strasbg.fr/Abstract.html

⋆⋆⋆ *Permanent address:* Instituto Astronômico e Geofísico (IAG), Universidade de São Paulo, Av. Miguel Stefano 4200, 04301-904 São Paulo, Brazil.

from a state in which the high excitation lines are at maximum intensity, which we call a *high state* spectrum, to a complete disappearance of the high excitation lines, which we call a *low state* spectrum. We prefer such a purely phenomenological description of the spectrum because it is not proven that the mechanism that governs the spectroscopic events is the ejection of a shell by the star.

The prediction and successful observation of a spectroscopic event in 1998.0 (Damineli 1996; Abraham & Damineli 1997; Lopes & Damineli 1997; Jablonski et al. 1998) allowed the collection of huge amount of data in all electromagnetic energy windows. Critical constraints to models have been derived from observations ranging from X-rays to radio wavelengths. The presently known data favors the existence of a long period binary with wind-wind collision in the heart of the Homunculus (DCL; Stevens et al. 1997; Corcoran et al. 1997). Optical and near-infrared spectroscopy, however, hasn't been exploited at the level permitted by the techniques available in the last twenty years. Some published papers include high resolution or large spectral coverage but both characteristics have not been used at the same time (Hillier & Allen 1992; Meaburn et al. 1993; Damineli et al. 1993; Hamann et al. 1994). In particular, a systematic study of line parameters, separating the narrow and broad line components, has not yet been performed, although it is known that they are formed in regions of different physical characteristics. Davidson et al. (1995, 1997) have shown that the narrow components are formed mainly in slow-moving condensations about $0\farcs3$ from the star; see Sect. 6 below. In some important works, unfortunately, information from spectra of different dates have been analyzed together (Davidson et al. 1986; Hamann et al. 1994; Johansson et al. 1995), in spite of the known spectral variability. Even line identification (Aller & Dunham 1966; Viotti 1968; Thackeray 1969; Hamann et al. 1994) merits revision on the basis of higher resolution observations and new atomic transition calculations.

The purpose of our long-term survey is to improve the knowledge of η Car's spectrum at wavelengths accessible by CCDs through ground-based telescopes. In this particular work, we analyze the wealth of information that can be derived by comparing the spectrum on two extreme situations, the states of highest and lowest excitation, that occurred mid-1995 and mid-1992, respectively. A detailed study of the temporal variability will be reported in a separate paper.

2. Observations and data reduction

The ESO spectra were collected at the ESO 0.52-m telescope with the Heidelberg fiber-linked echelle spectrograph FLASH/HEROS (cf. Kaufer et al. 1996 and references therein). The spectra have a spectral resolution of about 20 000 with a fiber diameter of 100 μm, corresponding to $2''$ projected on the sky. The reduced spectra have been binned to 0.1 Å/pixel. The low state spectrum was obtained on 20 June 1992, exactly on the center of the 1992 spectroscopic event, and covers the spectral range $4040 - 6790$ Å. The low state spectrum is a combination of seven spectra in the blue ($3450 - 5540$ Å) and eight spectra in the red ($5800 - 8600$ Å). We averaged the 1995 spectra to enhance the signal-to-noise ratio (S/N), as no variability was detected at the time spanned by those observations.

LNA spectra were collected at the Coudé focus of the 1.6-m telescope with a 1152×750 GEC/CCD; the dispersion was 0.4 Å/pixel and the measured $fwhm$ of the comparison lamp was 0.7 Å. The slit width was close to $1''$. Several spectra were collected in the $3600-11000$ Å wavelength range, but only the subset of data complementary to the ESO (yellow and near-infrared) spectra are presented here. The low state spectra were collected on 3 June 1992 and the high state spectra on May 1995 at LNA observatory. Spectra collected on 20, 24, and 25 June 1992 show that some lines hadn't yet reached the very minimum in 3 June 1992. However, the differences are small and the spectral coverage at LNA was much more complete in 3 June 1992 than on mid-June, allowing spectra collected on that date to represent the low excitation phase to a reasonable approximation.

We degraded ESO spectra to 0.4 Å/pixel in order to compare it with that of LNA, collected in the same epochs. No measurable differences were found in the line profiles. Low resolution spectra collected at LNA on 24–31 May 1992 and 15–16 June 1992 (not reported here) confirm that that [Ne III] λ3868 line was absent on the low state spectrum. This is important information, as no high resolution spectrum shorter than 4000 Å was collected during the 1992.5 spectroscopic event.

ESO spectra were reduced with the MIDAS package and that of LNA with IRAF[1]. All line measurements were performed with the IRAF package installed on CASA computers (University of Colorado). After normalization of the spectrum to the continuum level, measurements of isolated lines and individual components inside blends were performed in the standard way. Extracting line parameters from η Car's spectrum is not a trivial task, because of asymmetries in the broad line components and lines with extended wings. Gaussian fit was adopted in all cases except for too complicated blends. For these, only the total flux is meaningful and integration under the normalized line profile was used. When measuring the low state spectrum, we always overplotted the high state spectrum, and vice-versa, in order to adopt the same criteria for both. Many training trials were done until a high degree of repeatability in the results was attained. These steps were crucial, as the criteria had to be kept

[1] IRAF is distributed by the National Optical Astronomy Observatories.

unchanged for months, during which many thousands of measurements were performed. The data presented here have a high degree of internal consistency. When comparing our measurements with that of other authors, however, care must be taken, as assumptions regarding the beginning and ending of the spectral features and the level of the continuum are likely to be different from one author to another.

3. A general view of the results

The optical and near-infrared (NIR) spectrum of η Car is very rich in emission lines, with ionization potentials of atomic species ranging from ~ 6 eV to more than 60 eV. It is a mixture of permitted and forbidden lines with narrow components ($fwhm \sim 20 - 80\,\mathrm{km\ s^{-1}}$) seated on ~ 8 times broader components. Hα is the strongest line, peaking at $I_{\rm peak}/I_{\rm c} \sim 200$ in high state, followed closely by He I λ10830. Single ionized iron shows the most numerous atomic transitions, with 20% more Fe II than [Fe II] lines, ranging from intermediate to low intensities. A group of highly excited lines ([Ne III], [Fe III], [Ar III], and [S III]) and some nitrogen lines also have intermediate strength. Numerous faint lines, mainly from Fe II, Ti II, Cr II and N I, make the spectrum of η Car very crowded, with plenty of blends and only a few regions free of lines to sample the real stellar continuum.

In Fig. 1, we present the spectrum from 4040 to 10970 Å, excluding the wavelength regions heavily affected by telluric absorption ($7200 - 8400$ Å and $8900 - 9900$ Å). In the upper part of figure, we display the high state spectrum (solid line) superimposed on the low state (dotted line). The intensity relative to the stellar continuum was transformed to a logarithmic scale, in order to enhance the visibility of the broad line components and their variations. The S/N in the stellar continuum is displayed for some wavelengths. Numbers above the spectrum plot are for 1995 and below for June 1992. We show $S/N \geq 100$ in the red region ($6000 - 7000$ Å) decreasing to $S/N \sim 20 - 40$ at the blue and near-infrared extremities. The S/N is higher in the emission lines than in the continuum, obviously. It is important to emphasize that photon noise is not the main source of uncertainty in the line measurements. Errors are dominated by the placement of the continuum level and by uncertainties in deblending the components.

The ratio between the 1995 and 1992 spectra is labeled *high/low* in Fig. 1 and is displayed in linear scale at the bottom of each plot window. It is useful for a quick look at line variability, line profiles and for guessing what component belongs to which transition. For example, in Fig. 1c, the [Fe III] λ4769 line is faint and blended, but the *high/low* plot shows a line profile very similar to the neighboring isolated [Fe III] λ4750, λ4701, and λ4654 lines. Similarity between lines of Balmer series is very clear in the *high/low* ratio plot, although difficult to see in the original spectrum because of blendings. Before dividing the 1995 and 1992 spectra, we performed a 5-point triangular smoothing to avoid spikes due to small wavelength mismatches. In this way, the *high/low* ratio plot tends to underestimate the real amplitude of variations from high to low states. The horizontal dashed-line in Fig. 1 (ordinate equal 1) indicates the level of unchanged features; points above this line indicate that the feature had higher flux (relative to the continuum) in high state than on low, and vice-versa. For example, a line that was strong in 1995 but faint in June 1992 generates a high peak in the *high/low* ratio. This is the case of P Cygni components that are deeper in low than in high state. A complete description of the features displayed in Fig. 1 will be presented in the next sections.

In Table 1, we present the measured line parameters. A short dash indicates that the corresponding measurement was not performed because it was meaningless or technically unfeasible. In *Column 1*, a number designates the sequential order in wavelength of a spectral line or blend of lines. Letters label individual features inside a blend. *Column 2* displays the identification of atomic transitions: *notidf* stands for not identified feature, an interrogation mark (?) for a doubtful identification, and IS indicates an interstellar absorption. *Column 3* comments on the appearance of the feature: *sgl* stands for a single isolated line, *comp* for an isolated transition composed with more than one component, *nar* for a narrow line component, *bro* a broad line component, *bld* for a blending of different atomic transitions, *P Cygni* for a blue shifted absorption, *pV* and *pR* for the violet and red components of a double-peaked line, *abs* for an absorption component superimposed on the emission profile, *bshd* for an enhancement of the blue extremity of the broad line component, *bem?* for a feature that looks like a blueshifted emission present in some lines, an exclamation mark (!) for a remarkable feature, and an interrogation mark (?) for doubt about the reality of the feature. As it is difficult to know a priori if a double-peaked line is produced by an absorption feature or by two emission components, we measured both the peaks and the valley. *Column 4* displays the laboratory wavelength of identified transitions (in Å); numbers inside brackets are the suggested laboratory wavelength for transitions where we didn't find a reliable identification. The suggested laboratory wavelength was obtained by shifting the measured line center by $+40\,\mathrm{km\ s^{-1}}$. *Columns 5* through *9* refer to the 1995 (high state) spectrum and *10* though *14* to 1992 (low state) spectrum. In *Columns 5* and *10* we present the observed wavelength barycenter of the line components (in Å), measured through Guassian fit; *Columns 6* and *11* the heliocentric radial velocity ($\mathrm{km\ s^{-1}}$); *Columns 7* and *12* the line peak intensity relative to the local stellar continuum; *Columns 8* and *13* the line flux normalized to the continuum (in units of Å)

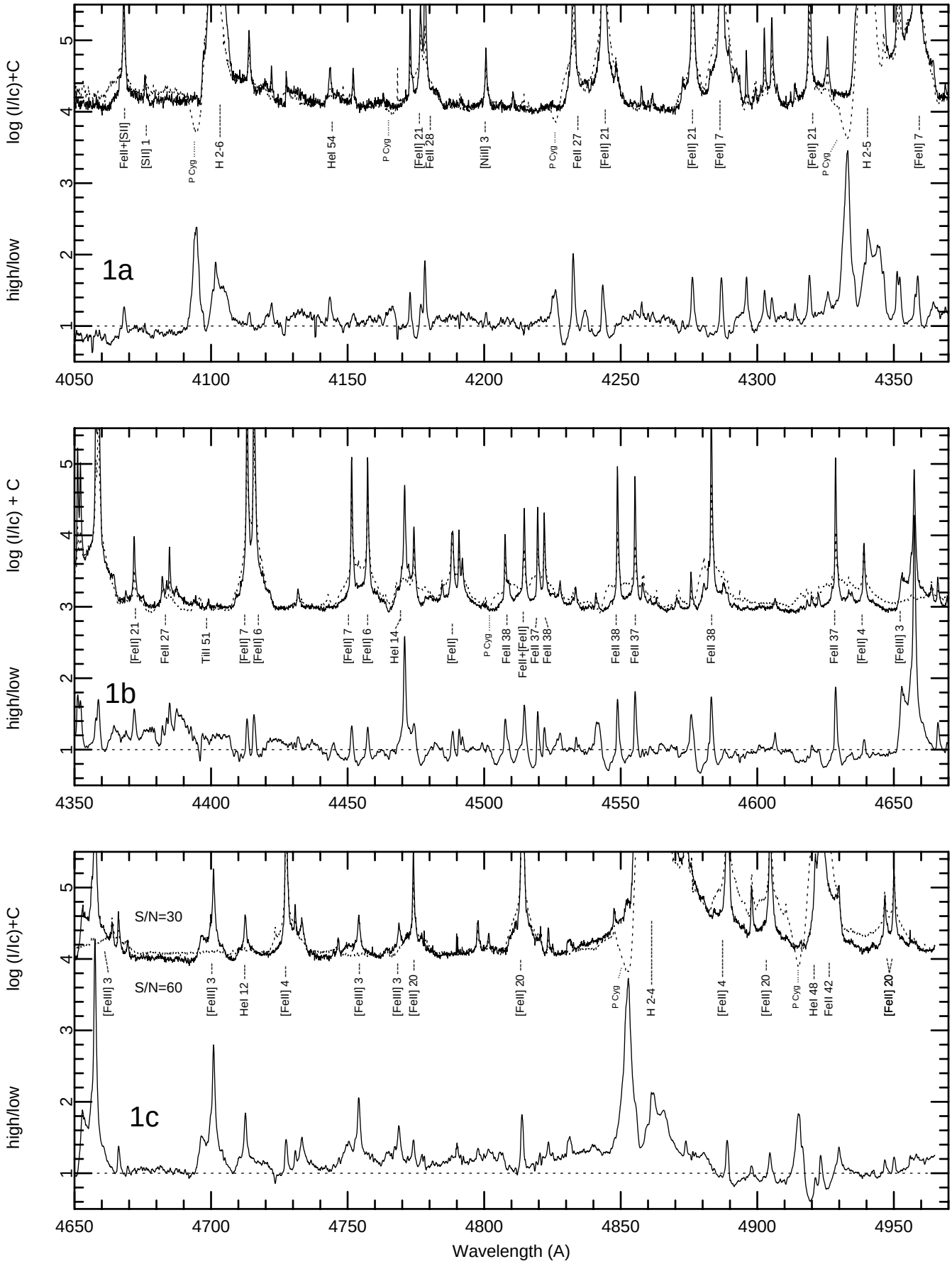
log (I/Ic)+C
high/low
1a
FeII+[SII] ---
[SII] 1 ---
P Cyg .....
H 2-6 ---------
HeI 54 ---
P Cyg .....
[FeII] 21 ---
FeII 28 ----
[NiII] 3 ---
P Cyg .....
FeII 27 -----
[FeII] 21 ----
[FeII] 21 ----
[FeII] 7 ---------
[FeII] 21 ---
P Cyg .....
H 2-5 ---------
[FeII] 7 ----
4050
4100
4150
4200
4250
4300
4350
log (I/Ic) + C
high/low
1b
[FeII] 21 ---
FeII 27 ---
TiII 51 ---
[FeII] 7 ---
[FeII] 6 ---
[FeII] 7 ---
[FeII] 6 ---
HeI 14 ---
[FeII] ---
P Cyg .....
FeII 38 ---
FeII+[FeII] ---
FeII 37 ---
FeII 38 ---
FeII 38 ---
FeII 37 ---
FeII 38 ---
FeII 37 ----
[FeII] 4 ---
[FeIII] 3 ---
4350
4400
4450
4500
4550
4600
4650
log (I/Ic)+C
high/low
1c
S/N=30
S/N=60
[FeIII] 3 ---
[FeIII] 3 ---
HeI 12 ---
[FeII] 4 ---
[FeIII] 3 ---
[FeIII] 3 ---
[FeII] 20 ---
[FeII] 20 ---
P Cyg .....
H 2-4 ----------
[FeII] 4 ---------
[FeII] 20 ---
P Cyg .....
HeI 48 ----
FeII 42 ----
[FeII] 20 ---
4650
4700
4750
4800
4850
4900
4950
Wavelength (A)

Fig. 1. **a**–**c**)

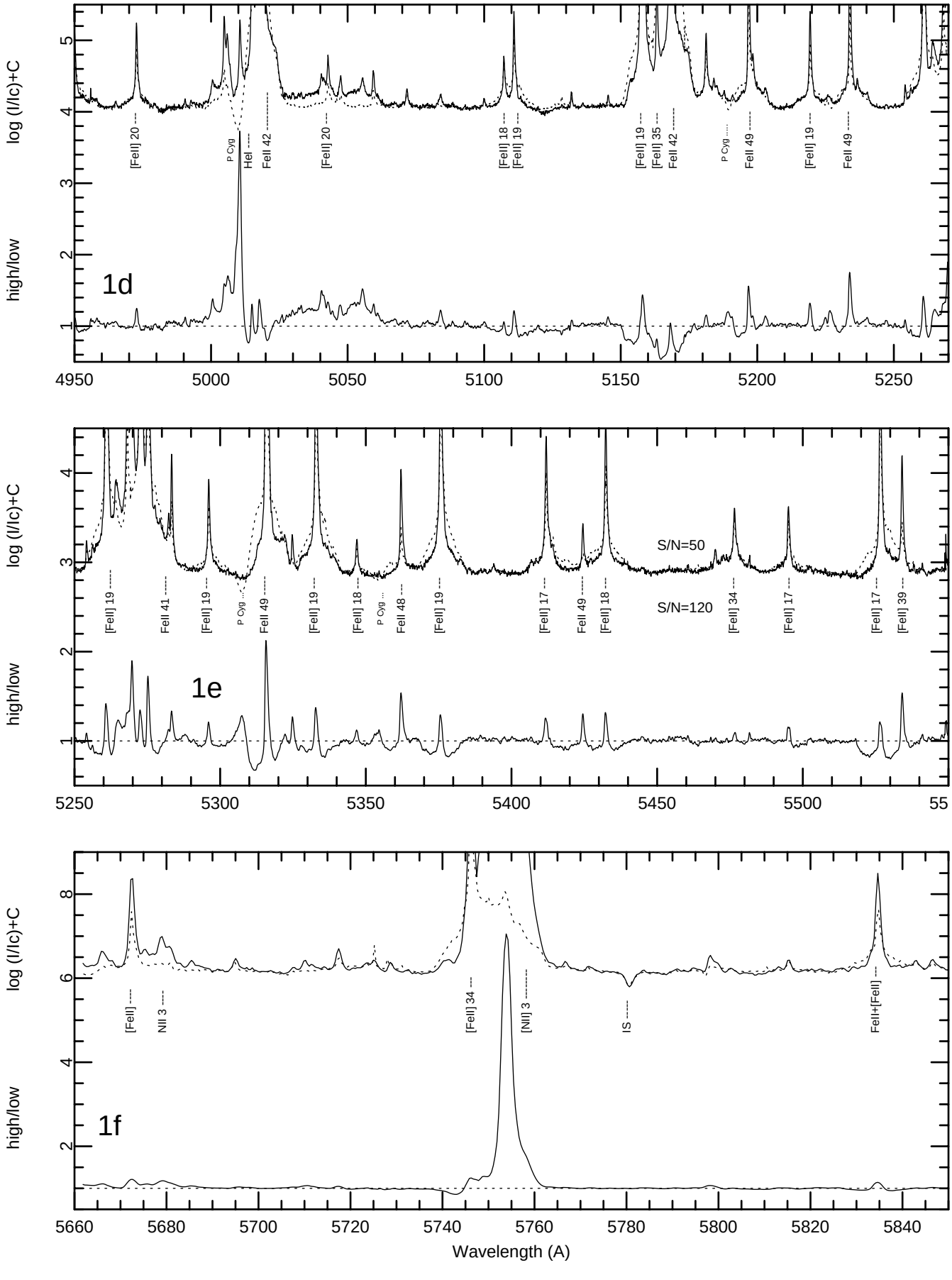
log (I/Ic)+C
high/low
1d
[FeII] 20
P Cyg
HeI
FeII 42
[FeII] 20
[FeII] 18
[FeII] 19
[FeII] 19
[FeII] 35
FeII 42
P Cyg
FeII 49
[FeII] 19
FeII 49
4950
5000
5050
5100
5150
5200
5250
log (I/Ic)+C
high/low
1e
S/N=50
S/N=120
[FeII] 19
FeII 41
[FeII] 19
P Cyg
FeII 49
[FeII] 19
[FeII] 18
P Cyg
FeII 48
[FeII] 19
[FeII] 17
FeII 49
[FeII] 18
[FeII] 34
[FeII] 17
[FeII] 17
[FeII] 39
5250
5300
5350
5400
5450
5500
55
log (I/Ic)+C
high/low
1f
[FeII]
NII 3
[FeII] 34
[NII] 3
IS
FeII+[FeII]
5660
5680
5700
5720
5740
5760
5780
5800
5820
5840
Wavelength (A)

Fig. 1. d–f)

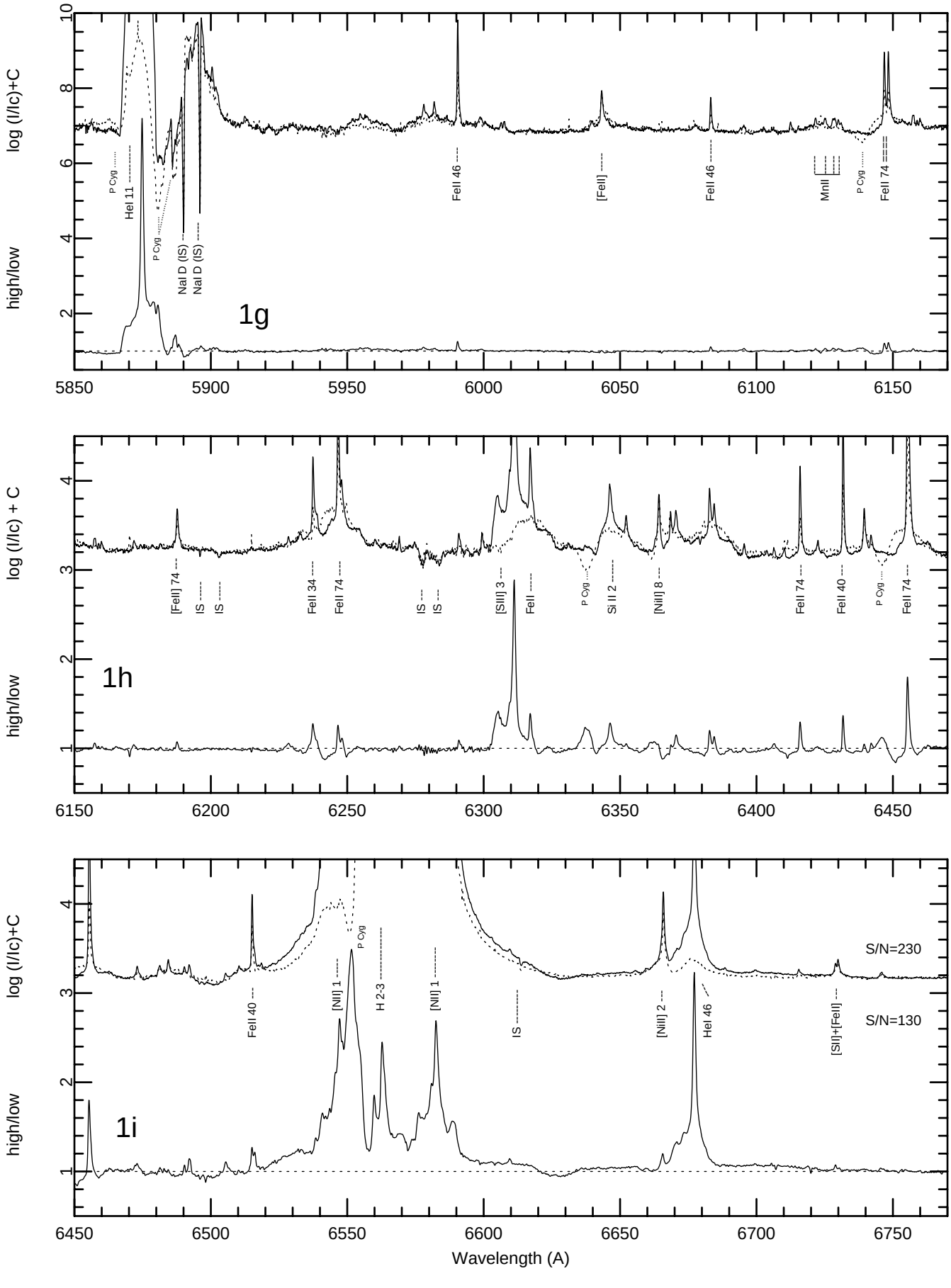
log (I/Ic)+C
high/low
P Cyg
HeI 11
P Cyg
NaI D (IS)
NaI D (IS)
FeII 46
[FeII]
FeII 46
MnII
P Cyg
FeII 74
1g
5850
5900
5950
6000
6050
6100
6150
log (I/Ic) + C
[FeII] 74
IS
IS
FeII 34
FeII 74
IS
IS
[SIII] 3
FeII
P Cyg
Si II 2
[NiII] 8
FeII 74
FeII 40
P Cyg
FeII 74
1h
6150
6200
6250
6300
6350
6400
6450
log (I/Ic)+C
FeII 40
[NII] 1
P Cyg
H 2-3
[NII] 1
IS
[NiII] 2
HeI 46
[SII]+[FeII]
S/N=230
S/N=130
1i
6450
6500
6550
6600
6650
6700
6750
Wavelength (A)

Fig. 1. g–i)

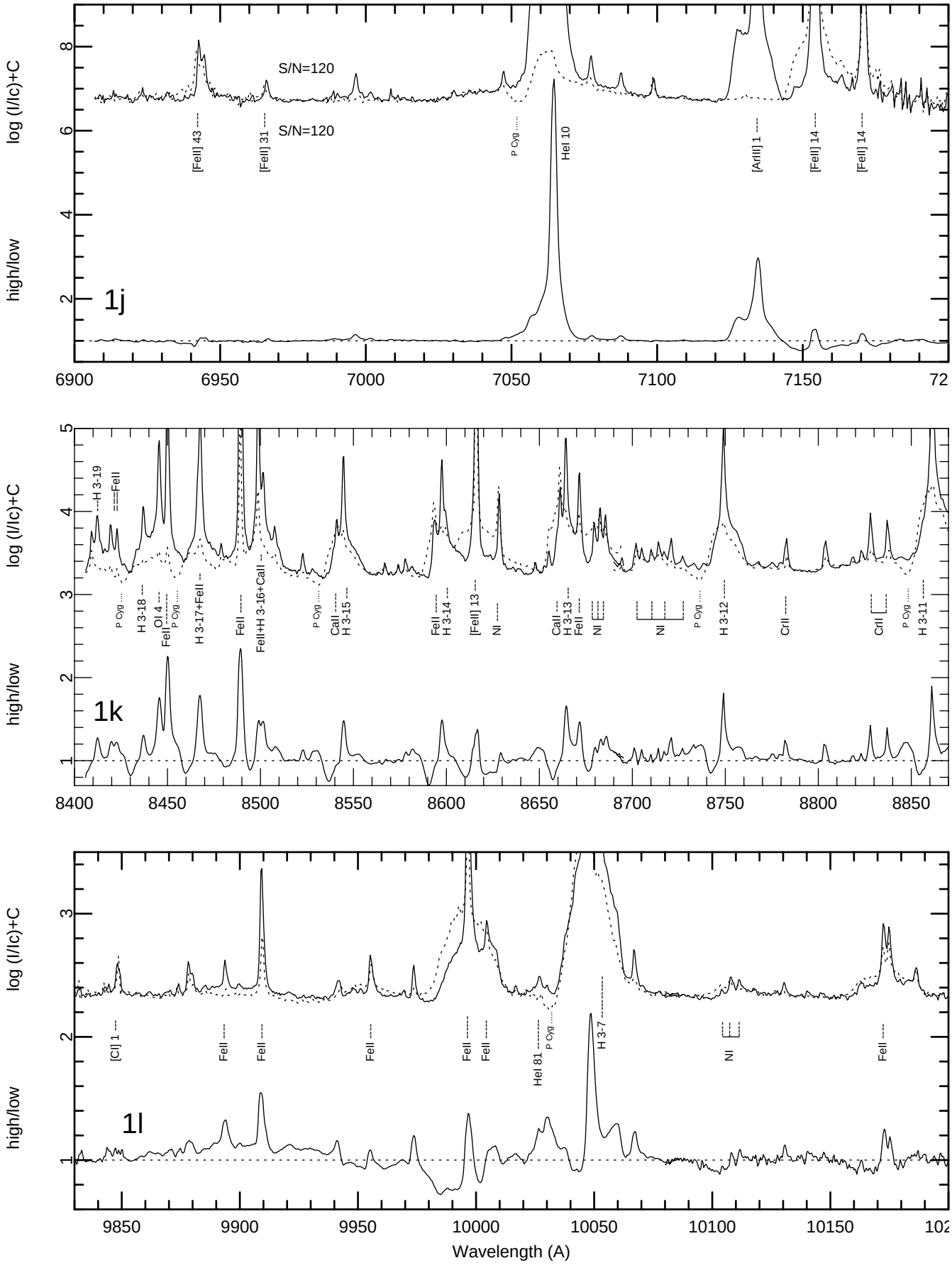
log (I/Ic)+C
high/low
S/N=120
S/N=120
[FeII] 43
[FeII] 31
P Cyg
HeI 10
[ArIII] 1
[FeII] 14
[FeII] 14
1j
6900
6950
7000
7050
7100
7150
H 3-19
FeII
P Cyg
H 3-18
OI 4
FeII
P Cyg
H 3-17+FeII
FeII
FeII+H 3-16+CaII
P Cyg
CaII
H 3-15
FeII
H 3-14
[FeII] 13
NI
CaII
H 3-13
FeII
NI
NI
P Cyg
H 3-12
CrII
CrII
P Cyg
H 3-11
1k
8400
8450
8500
8550
8600
8650
8700
8750
8800
8850
[CI] 1
FeII
FeII
FeII
FeII
FeII
HeI 81
P Cyg
H 3-7
NI
FeII
1l
9850
9900
9950
10000
10050
10100
10150
Wavelength (A)

Fig. 1. j–l)

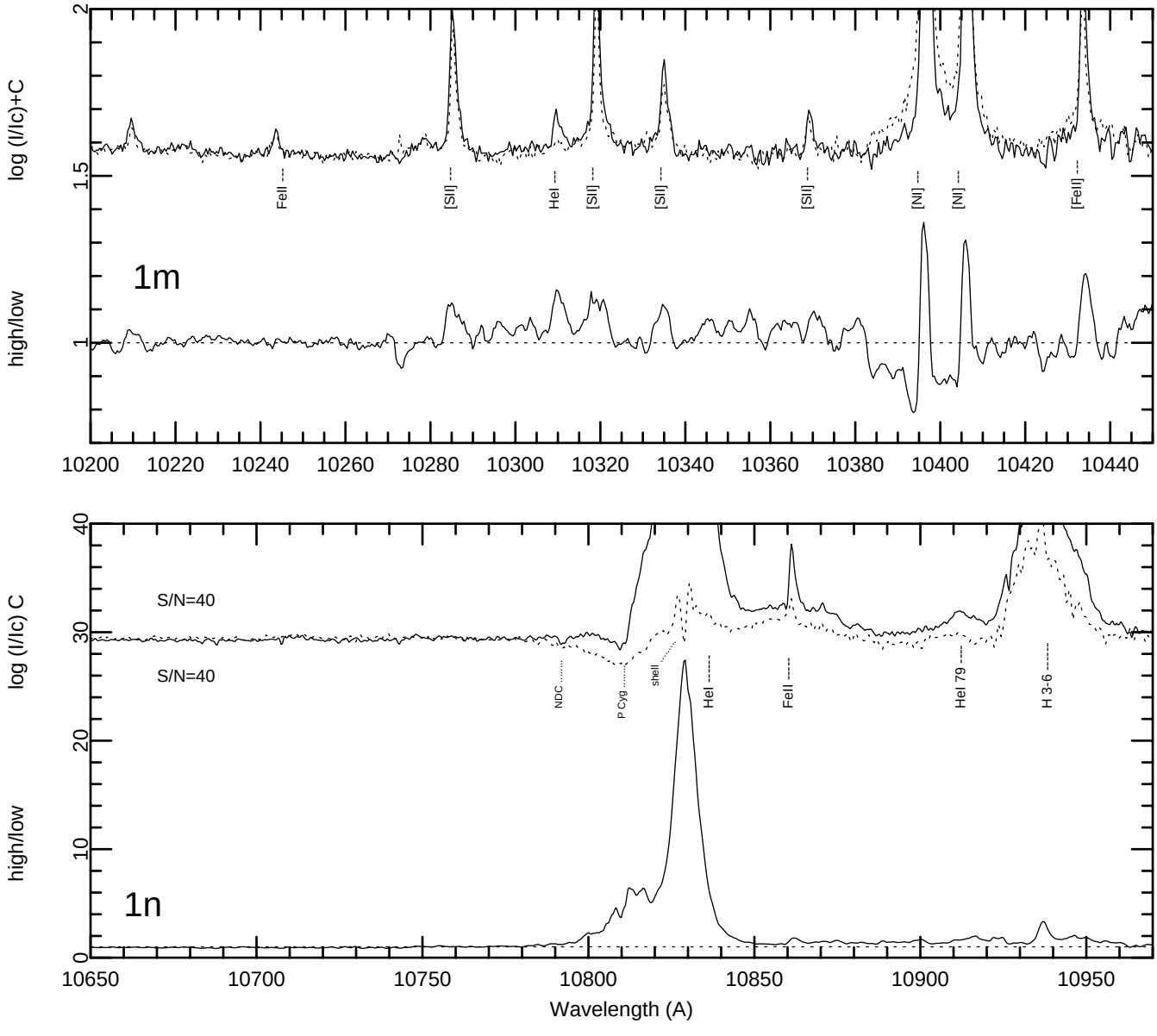

Fig. 1. m–n)

Fig. 1. a–n) The solid line at the top of each panel represents the high state spectrum and the superimposed dashed line the low state spectrum. The scale is logarithmic to enhance the broad line features. The ratio between the two spectra *high/low*, is plotted at the bottom, in linear scale

- this coincides with the classical definition of equivalent width when the base of the line merges into the local continuum. A minus sign in *Columns 7, 8, 12* or *13* indicates that the feature in absorption. In *Columns 9* and *14* we present the $fwhm$ of the feature (in km s^{-1}), corrected for the instrumental profile. *Column 15* displays the percent variation of the line flux, relative to that in 1995 (high state), derived from the expression:

$$var \; = \; 100\,\frac{\mathrm{flux}_{1995} - \mathrm{flux}_{1992}}{\mathrm{flux}_{1995}}. \qquad (1)$$

A line that fades completely during the low state results in a number 100 in *Column 15*, while negative numbers are for lines that are stronger on that phase than in low state. P Cygni components result in largest negative numbers in *Column 15*, as most of them were faint or absent in 1995. In order to not have an undetermined value in *Column 15*, we adopted a flux of -0.1 in *Column 8* when the feature could not be measured reliably in the 1995 spectrum.

The way we defined the index of variability (*var*) in *Column 15* of Table 1 is analogous to the *high/low* ratio plotted in Fig. 1. The main differences between the two ways of defining variability of the spectral features are: a)

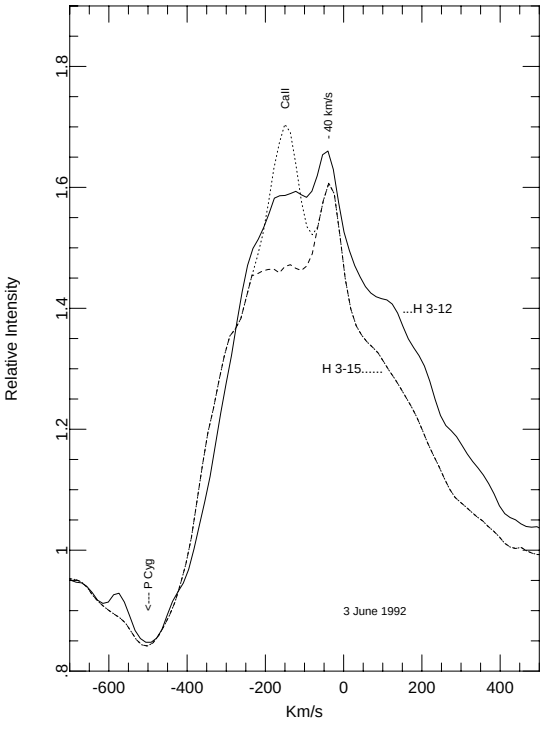

Fig. 2. The Ca II λ8542 Å line is represented by a dotted line, blended with H 3-15. The Paschen-15 line after deblending (dashed line) shows the same line profile as Paschen-12 (continuous line)

a nonvariable feature results in $var = 0$ while $high/low = 1$; b) variations in the P Cygni profiles result in $var \leq 0$ while $high/low \geq 0$. The advantage of the *var* parameter over the *high/low* ratio is that it doesn't depend on the line intensity, allowing a direct comparison of the degree of variability between strong and faint lines. Unfortunately, the *high/low* ratio couldn't be defined in the same way, as it would result in a very noisy plot, disabling the evaluation of variability by a quick look.

4. Line identification

The first step in the process of line identification is to match observed with laboratory wavelengths. This can be done once the radial velocity of each feature is known. By using 200 lines well-identified in previous works, we derived a radial velocity of $rv = -40 \pm 5\,\mathrm{km\ s^{-1}}$ for the centroid of the narrow line components (radial velocities are in heliocentric system through this paper, as indicated in Sect. 3). This is in excellent agreement with results of Zanella et al. (1984) who obtained $rv = -40 \pm 2\,\mathrm{km\ s^{-1}}$. High spatial resolution observations with the HST show that this is the velocity of the discrete "Weigelt blobs" near the star (Davidson et al. 1995, 1997). The uncertainty of present data, $\sigma = 5\,\mathrm{km\ s^{-1}}$, is larger than derived by Zanella et al. in spite of our larger spectral dispersion, more numerous lines, and broader spectral coverage. This indicates that there is a real scatter in radial velocity between the emitting clouds.

We shifted the observed line wavelengths by $+40\,\mathrm{km\ s^{-1}}$ to derive the expected laboratory wavelengths displayed in *Column 4* of Table 1. We searched for candidates of atomic transitions in the works of Hamann et al. (Aller & Dunham 1966; Thackeray 1967, 1969; Viotti 1968; Hamann et al. 1994; McKenna et al. 1997; and in the unpublished Fe II oscillator strengths of Kurucz. Candidate transitions were rejected if departing more than $3\,\sigma$ ($= 15\,\mathrm{km\ s^{-1}}$) from the average radial velocity ($rv = -40$ km s^{-1}). Several suggested identifications in previous papers were ruled out. We searched carefully for [O II], [O III], and He II and found no traces, definitively rouling out the presence of these lines in the central knot of η Carinae. A complete identification of the measured features is out of the scope of the present work. However, as too many lines remained unidentified in our list, we felt compelled to provide as much new information as possible.

The second step in the process of identification was to compare the strength of the candidate transition to what should be expected from other well known lines. This is very important in the case of ions rich in transitions, such as Fe^{+}. We identified new lines of [Fe III], [Fe II], Fe II, N I, [N II] Si II, and Ca II. The line [S II] λ4068 is much stronger than expected from the intensity of [S II] λ4076 (Fig. 1a). In fact, a Fe II transition in the Kurucz semiempirical list was found to be blended with [S II] λ4068, what excludes this line for reddening measurements in the method proposed by Rodgers & Searle (1967). The [S II] λ 6729 line was too strong, compared to [S II] λ 6716, and we found it to be blended with a Fe II line. After deblending and measuring the ratio between the two [S II] lines, we derived a density of $1.2 \pm 0.410^4\,\mathrm{electrons\,cm^{-3}}$ for the narrow line region, which is substantially lower than those derived by other authors (Hamann et al. 1994 and references therein). The infrared Ca II triplet was expected to be detected, due to the presence of Mg II, Na I, N I, Fe II, and other Ca II and [Ca II] lines in the spectrum of η Car and similar objects. The identification, however, was tricky, because an unfortunate sequence of blends in the Paschen lines produces an impression of double-peaked profiles in the higher members of the series (Fig. 1k). Actually, the false double peaks disappeared abruptly in Paschen lines at wavelengths longer than H 3-12 and are not shown in H 3-18 and H 3-17.

A third step in identification was to look for variability in the line between the high and low states and to compare it with other lines of the same ion. For example, in the case of the infrared Ca II triplet, the false violet peaks in H 3-15 and H 3-13 didn't fade in low state (Fig. 2). As can be seen in Fig. 1k, the red line peak disappears in

low state in H3-18, H3-12, and H3-11, and in the higher members of Balmer series. After deblending from the proposed Ca II line, H 3-15 shows a narrow component at $-40\,\mathrm{km\,s^{-1}}$ seated on a broad component, a line profile very similar to H 3-12, as seen in Fig. 2. Another example is that of Ti II lines. Almost all lines of this ion are stronger on low than in high state, so only candidates behaving in the same way were accepted as reliable Ti II. In the same scheme, highly variable Ni II candidates were ruled out. Variability in the broad line component is also a powerful tool for confirming the identification of some features. For example, the enhancement of the broad component in the line at 4068 Å in low state confirms that the the line in blending is very probably from Fe II. Another important line for diagnostic, [N II] λ5755 (Fig. 1f), also clearly shows the presence of [Fe II] λ5747 in blending, when looking at variability from high to low state. Several lines in Table 1 have an interrogation mark in *Column 2*, because showing variability discrepant from the majority of other lines of the same ion, as is the case of: Ti II λ4307.90; [Fe II] λ4533.00, λ4664.45, λ4792.28, λ5900.51, λ6043.16, λ6044.16, λ6944.91, and λ6966.32; Fe II λ4666.75, λ4670.17, λ8595.19, and λ10245.58; Cr II λ4558.66 and λ4571.24; [Ni II] λ6007.30; and N I λ6008.48. However, because these lines are faint and may be affected by measurement errors or unknown blends, the correct identification is still pending. We suggested N II as possible identification for the lines at 5676.02, 5679.56, and 5686.21 Å based on wavelength coincidence, the presence of these lines in the spectrum of the star P Cygni, the presence of other N^+ transitions in η Car, and the disappearance of the narrow component in low state which is typical of high excitation lines.

The previous identifications of Sc II λ5667.16, [V II] λ6040.31, and [O I] λ6300.23 are doubtful, because they were based only on wavelength coincidence. Regarding the former two lines, it is unlikely that these ions show only one transition each across the entire optical/NIR spectrum. For [O I] λ6300, the identification seems suspicious because the expected stronger [O II] and [O III] are completely absent from η Car's spectrum.

We did not revise the identifications of Cr II, [Cr II], and [Co II] lines. Only a few faint [Cr II] and [Co II] lines are present in η Car's spectrum. In addition to matching the observed wavelengths, the Cr II lines proposed in earlier works show a coherent variability from high to low state, indicating that the identifications in previous works should be correct.

The identification of some features, such as *P Cygni* profiles, shoulders, absorption components, and double peaks, is a complex procedure and involves the comparison of several lines of related transitions of the same ion. The basic criteria are: the consistency in radial velocities, variability pattern from the high to low state, and broadness of the feature. P Cygni profiles generally drop below the level of the stellar continuum, have large radial velocities, and are much stronger in low then in high state spectrum, except for Ca II and Na I D lines. The *high/low* ratio plot is a powerful tool when used to identify P Cygni components. As can be seen in Fig. 1, H and Fe II lines (multiplets 27, 28, 42, 49, 74) present prominent features in the *high/low* plot at positions corresponding to P Cygni components. Relatively narrow lines appear on the blue edge of P Cygni components in some H lines. No identification was found for them and we labeled these features *bemis?* in Table 1, as they seem to be emission components blueshifted by -600 to $-760\,\mathrm{km\,s^{-1}}$. In some lines the blue-displaced *absorption* components is superimposed on the emission profile. The largest number of these features is shown by Na I. Many of them are likely to be multiple P Cygni components, but we cannot exclude that some may be valleys in between multiple emission components. In the case of He I λ10830 and some Balmer lines, we also measured the individual peaks, labeled by pV and pR in Table 1, in spite of the fact that we do not favor the interpretation of these features as real emission. High excitation lines show a *shoulder* in the blue edge of the broad component, which has been attributed to independent transitions in some previous works. For example, the feature at 6305 Å (Fig. 1i), previously identified as Fe II 200, faded together with the narrow component of [S III] λ6312, indicating that it is a part of the [S III], rather than an independent line. This is confirmed by the line profile of other high excitation lines.

5. Line strengths in high and low states

Line flux variability in the η Car spectrum seems complicated, at first glance. However, it follows a simple general pattern: the higher the excitation level of the transition, the higher the fading of the line in low state. Some of the lowest excitation lines are several times stronger during low state than in high state. For intermediately excited lines, the narrow component suffers strong fading in low state but the broad one fades by a lower extent. We will describe with more detail the strongest and less blended lines of each atomic species. Variations in the line flux are plotted in Fig. 3. In that figure, the x-axis represents the line wavelength and the y-axis the *var* parameter defined in Eq. (1) and displayed in *Column 15* of Table 1. In Fig. 3, large symbols label broad components, small symbols the narrow components, and intermediate size symbols label the lines without separation between the components.

5.1. High excitation forbidden lines

The lines of [Ne III] λ3868; [Fe III] λ4658, and λ4701; [N II] λ5755, λ6548 and λ6583; [S III] λ6312; and [Ar III] λ7135 have the largest excitation levels in the optical/NIR wavelength range. On high state, the flux ratio is *broad/narrow*

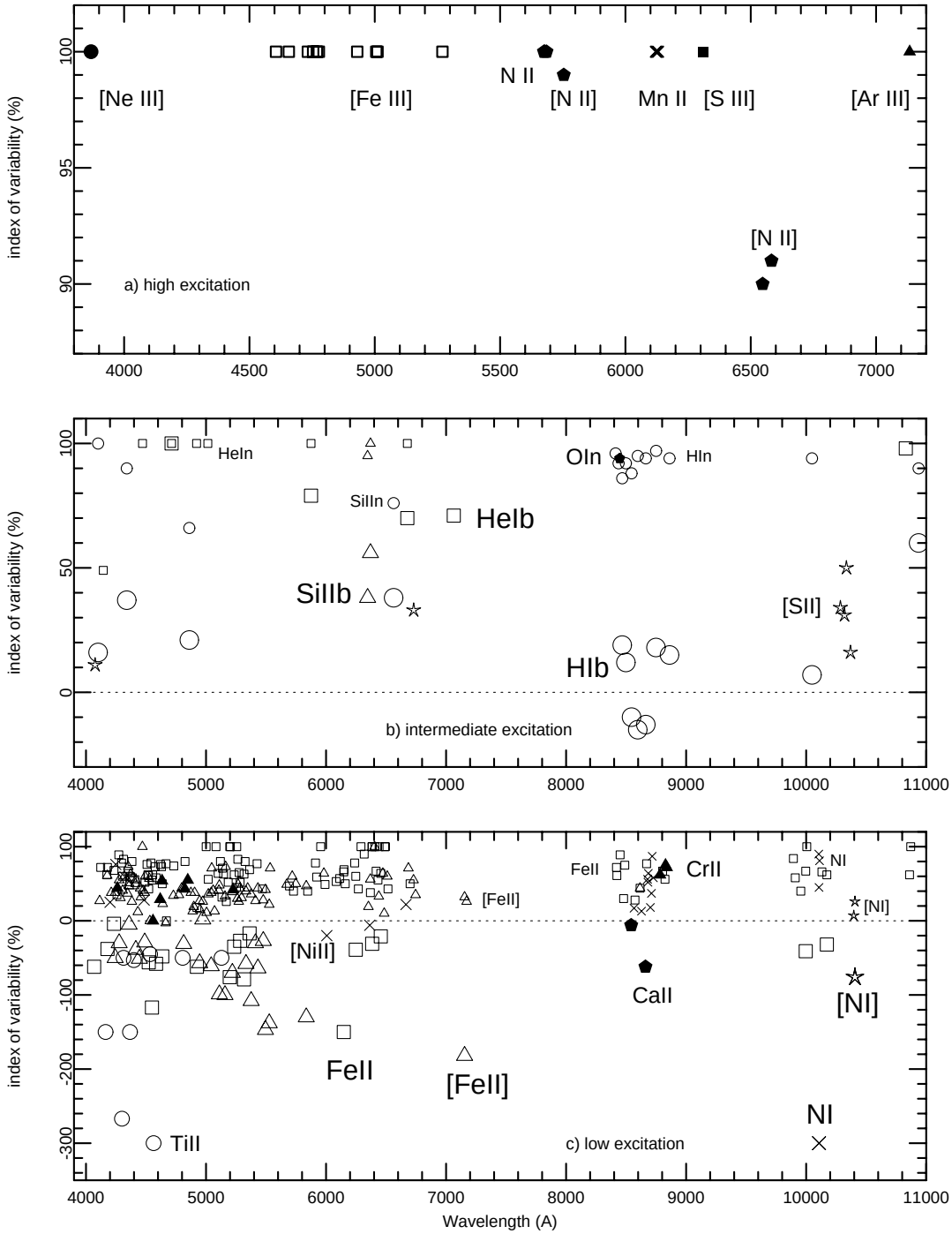

Fig. 3. Index of variability *var* as defined by Eq. (1). Panel **a)** shows the high excitation lines, panel **b)** intermediate excitation lines and panel **c)** the low excitation lines. Large symbols are for broad line components, small symbols for narrow components and intermediate symbols for lines in which the components were measured together (as high excitation lines, for example)

$\sim$2.3 and both components disappear completely during the low state (Fig. 3a). Lines of [N II] λ5755, λ6548, and λ6583 do not show a complete fading on the low state, because of contamination by blends. We plotted Mn II lines together with the high excitation lines because Mn II are excited by Lyα fluorescence (Johansson et al. 1995).

5.2. Neutral helium lines

The He I lines in high state show line profiles similar to that of the highest excitation lines. They have smoother blue shoulders and a little larger flux ratio: *broad/narrow* $\sim$2.6. On the low state, the narrow component disappears completely and the broad components suffer strong fading (Fig. 3b). He I λ10830 show a spectacular behavior, ranging from a strength similar to that of Hα in high state to almost disappearance in low state. The luminosity in this single atomic transition varies from 3000 $L_\odot$ to $\sim$15 $L_\odot$ from high to low state. The real figures would be larger, if redening was taken into account. This line is fed by UV continuum and, in other LBV stars, a decrease in the level of line excitation is correlated with a reddening in the color indices and, consequently, a brightening of the star in the optical range. The behavior of η Caris completely different: the luminosity in the continuum and color indices remain almost constant when lines vary by a factor of 14 000% in He I λ10830, showing that the spectroscopic events are not due to S Doradus variability. This line is a privileged one for timing the 5.52 year cycle and tracing its physical nature. Although it is easily detectable by normal CCDs at high spectral resolution, it hasn't received much attention from observers until now.

5.3. Neutral hydrogen lines

The H I lines have intermediate excitation levels and show a rich pattern of variability. Paschen lines exhibit the typical broad and narrow components with a flux ratio *broad/narrow* $\sim$ 3.8 in high state. The strength of the narrow components increases toward longer wavelengths. On low state, the flux ratio jumps to *broad/narrow* $\geq$ 50, mainly due to the fading of the narrow component as the strength of the broad one changes a slightly (Fig. 3b). For Balmer lines, an absorption component is superimposed on the narrow emission seen in Paschen lines, as described in the next section.

5.4. Fe II *and [*Fe II*] lines*

Many Fe^+ lines show very strong narrow components relative to the broad ones. On high state, the flux ratio is *broad/narrow* $\sim$1.3. On low state, this ratio grows to *broad/narrow* $\sim$4. This is due to a combined effect by which the broad components become stronger in low state and the narrow components become fainter. The fading of the narrow component in Fe II ($var = 80 \pm 20$) is more pronounced than that of [Fe II] ($var = 36 \pm 12$). The strengthening of the broad components changes in the opposite way: $var = -47 \pm 20$ for Fe II and $var = -116 \pm 93$ for [Fe II], as can be seen in Fig. 3c.

Several Fe^+ lines, however, show a pronounced narrow line component, relative to the broad one, and much larger variations from high to low state. For example, Fe II λ8490, has a very strong narrow component in high state that disappears almost completely in low state. This line is thought to be excited by fluorescence from Lyα photons (Johansson & Hamann 1993). The Fe II $\lambda\lambda$2508$-$10 lines are also excited by the same mechanism and disclosed large variations in the 1981 spectroscopic event (Viotti et al. 1989). This suggests that other Fe^+ lines that follow the same kind of pattern could also be powered by fluorescence. The Fe II λ9997 line does not show a particularly strong nor variable narrow component, in spite of being thought to be excited by Lyβ fluorescence. This suggests that fluorescence is not operative for Fe II λ9997 or that complicate radiation transfer effects are involved.

5.5. Other lines

The Si II λ6347 line behaves like hydrogen Paschen lines (Fig. 3b). In high state, the flux ratio is *broad/narrow* ~ 4 and in low state *broad/narrow* ≥ 50. The N I and [N I] lines resemble Fe IIand [Fe II] lines (Fig. 3c). The broad/narrow flux ratio in neutral nitrongen lines, however, is smaller than that in typical Fe II lines. The N I narrow line fluxes in low state are $\sim$50% lower than the flux in high state. The [N I] lines, however, remain almost at the same level and both N I and [N I] have enhanced broad components in low state.

The Ni II λ6666 line is representative of the other Ni II lines. The total energy flux in this lines decreases a little from high to low state in the same way as Fe^+ broad lines (Fig. 3c). The broad component of Ni II is difficult to separate from the narrow one and the flux ratio is *broad/narrow* ~ 1.2 in high state and *broad/narrow* ~ 1.6 in low state. The narrow component is fainter in low than in high state, which indicates that the broad component may be constant or become a little stronger in low state, as Fe II lines (Fig. 3c).

The Ti II lines are faint in η Car spectrum but strengthen remarkably in low state, as can be seen in Fig. 3c ($var = -100 \pm 70$). The broad line components are very faint in our spectra. However, based on the fact that in all other lines the narrow component is fainter in low than in high state, we infer that the Ti II broad components strengthen in low state. This kind of variability

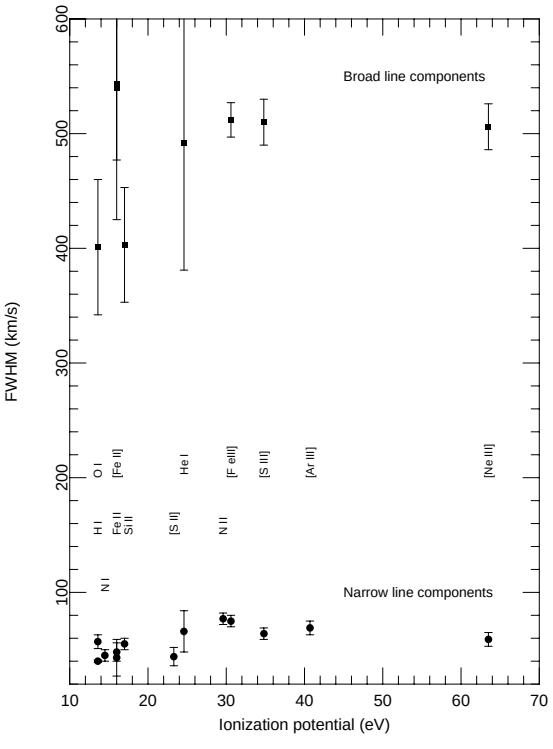

Fig. 4. Full width at half maximum ($fwhm$) of broad and narrow line components as a function of ionization potential. It seems to be a trend for lines belonging to ions of ionization potential lower than 30 eV to be narrower than for ions of higher ionization potential

reminds us of that seen in Fe II lines of multiplets 42, 48, 49, 74 etc., but with larger amplitude from high to low state. It is intriguing that many old papers described Ti II line profiles in some detail while it was painful to get even equivalent widths from our spectra. Are Ti II lines fainter today than several decades ago? This seems not to be the case, as the strengths of several other lines (He I λ4471, He I λ5876, [N II] λ5755 and Fe II) in high state seems to have been unchanged through all this century. It is not expected that only Ti II lines have varied. Our guess is that the S/N ratio in our CCD spectra is lower than were in photographic spectra in the blue spectral region.

Only the narrow component is seen in Cr II lines and they show smaller line strengths in low than high state, similar to the narrow components of Fe II lines.

The Na I $\lambda\lambda$5890/5 lines do not show the narrow component, a rarity in η Car's spectrum. The line flux is difficult to measure because of blending with HeI 5876 Å, but almost no variation is seen when superimposing the high and low state spectra.

The only oxygen line with firm identification in our spectra is O I λ8446 (O I λ7776 was not observed in 1992 and will not be discussed here). Only the narrow component can be seen in the blend involving H I, O I, and Fe II lines. This line suffers a huge fading in low state. It might even disappear completely in the central phase of the event. The [O I] λ6300 is not a reliable identification for the line at 6299.49 Å, as discussed previously.

The Ca II lines are also difficult to measure because of severe blends. The H and K lines in the blue spectral region show only P Cygni components. The narrow components in two members of the NIR triplet are definitively present and they seem to be constant or possibly a little enhanced in low state (Fig. 3c).

6. Velocity field

There are three main kinds of features in the η Car spectrum: the narrow components, with radial velocity $rv = -40 \pm 5\,\mathrm{km\ s^{-1}}$ and $fwhm \sim 60\,\mathrm{km\ s^{-1}}$; the broad components with $fwhm \sim -480\,\mathrm{km\ s^{-1}}$ and a large range of values in radial velocity; and P Cygni components with $rv = -330$ to $-630\,\mathrm{km\ s^{-1}}$ and $fwhm \sim 60$ to $600\,\mathrm{km\ s^{-1}}$. Figure 4 displays the $fwhm$ of narrow and broad line components as a function of the ionization potential of the ions. There is a trend for lines belonging to ions of ionization potential lower than 30 eV to show lower $fwhm$. The effect is more clear in narrow than broad line components.

Narrow lines do not show measurable changes in radial velocity or $fwhm$ from high to low state. The small dispersion in radial velocity indicates that all narrow lines are formed in the same region, in spite of the large ranges in energy levels. Davidson et al. (1997), using HST high spatialy resolved spectra, showed that narrow lines are formed in the nebular region $\sim$0.″3 from the central star, containing the Weigelt blobs (Hofmann & Weigelt 1988). These authors also showed that broad emission lines are restricted to the central knot. Broad permitted lines are formed in the stellar wind, but it's not clear if the broad forbidden lines can be formed in the wind too. The P Cygni components are formed in regions where the stellar wind apparently didn't yet reach terminal velocity. Several absorption structures, ranging from -130 to $-1350\,\mathrm{km\ s^{-1}}$, appear in different lines, indicating that the velocity field around the star is quite complex. P Cygni components of H I, Fe II, Si II, and N I lines show large increase in radial velocity from high to low states (Fig. 5). This does not necessarily imply variation of the wind flow parameters, as discussed later.

High excitation forbidden lines are on average a little broader than others. The narrow components have $fwhm \sim 70\,\mathrm{km\ s^{-1}}$ and the broad ones $fwhm \sim 510\,\mathrm{km\ s^{-1}}$. The radial velocity of the narrow components is similar to all other narrow lines, but the broad component has velocity $rv \sim -150\,\mathrm{km\ s^{-1}}$ that is blueshifted compared to the

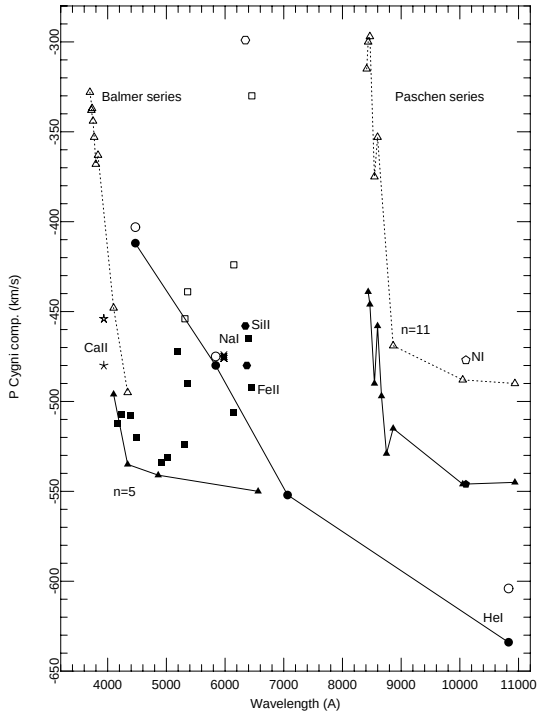

Fig. 5. Radial velocities of P Cygni components. Velocities are larger in low state (filled symbols) than in high state spectrum (open symbols) for H I, Fe II, Si II, and N I lines. Higher members of the Balmer and Paschen series are formed in a zone of rapid acceleration

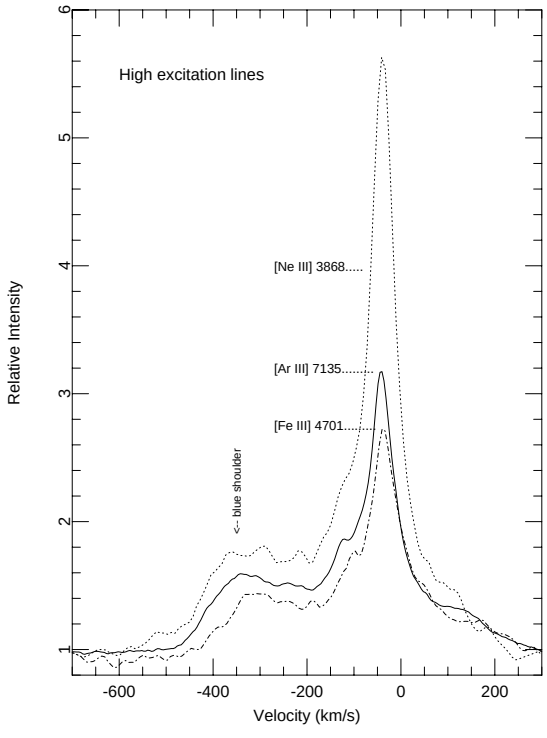

Fig. 6. Line profile of typical high excitation transitions. The broad components are centered at ~ -150 km s^{-1}, compared to the narrow ones, which are centered at -40 km s^{-1}

same feature in lines of lower excitation. The broad components of the high excitation lines have a remarkable line profile (Fig. 6). By subtracting the contribution of the narrow component, what remains is an asymmetric line with a distinctive emission at the blue side, $rv \sim -330$ km s^{-1} (labeled *bshd* in Table 1) and a fainter shoulder at the red side. Rather than extinction by dust, as suggested by Hamann et al. (1994), this kind of line profile seems to be produced by true anisotropy in the velocity field. The higher the ionization level of the ionic species producing the line, the broader are the line components. The broad component in high excitation lines doesn't change in radial velocity or line profile from high to low state, contrary to H, He I, and some Fe II lines. This indicates that the broad components of high excitation lines are unlikely to be formed in the stellar wind. Present data are insufficient to decide if this third emitting region is bound to the central knot or to the surrounding nebular region. Spectroscopy at radio wavelengths (Duncan et al. 1997) revealed high speed ionized gas in the region containing the Weigelt blobs. Davidson et al. (1997) didn't analyze high excitation forbidden lines and so, presently, we can't exclude that broad components of this type of lines can be formed outside the central object.

There are different line profiles for different He I lines. All He I lines show radial velocity variations in the broad component from high to low state. The amplitude of radial velocity variations are larger than in any other lines, but the separation between the broad and narrow component is difficult to measure in high state. The P Cygni components are stronger on low than high state, but without changing radial velocity. The He I λ10830 line has a unique line profile through all the η Car spectrum (Fig. 7). He I λ10830 shows an absorption feature at $rv = -50$ km s^{-1}, a little more negative than the narrow emission component. It is actually a shell absorption, as it is narrow, $fwhm = 30$ km s^{-1}, and the line center drops below the continuum level on low state. No radial velocity nor $fwhm$ variation was seen from high to low state in the shell component. This feature indicates the existence of high density, low velocity gas in front of the star, in the line-of-sight towards the Earth. The high velocity components are formed in the wind. During low state, He I λ10830 shows a remarkable P Cygni profile, centered at $rv = -630$ km s^{-1} and extending to more than -1400 km s^{-1}. By adopting the criterium that terminal

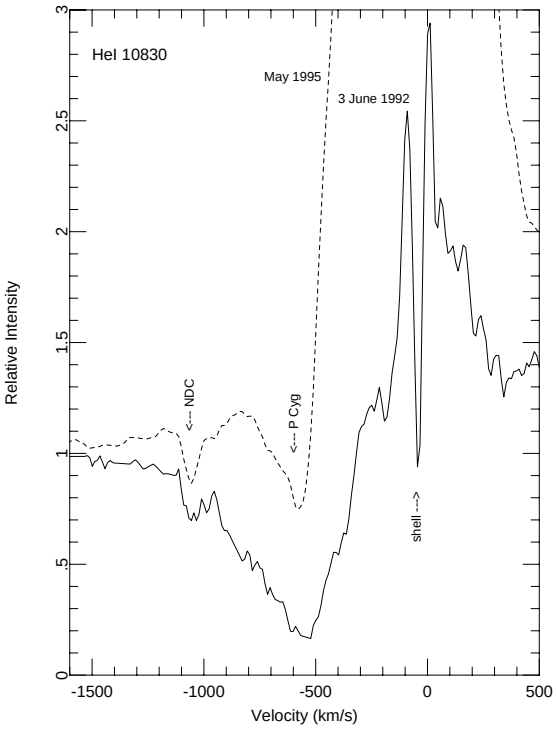

Fig. 7. Line profile of the He I λ10830 in high (1995) and low excitation phases (1992). The absorption features indicated as NDC ($-1061\,\mathrm{km\ s^{-1}}$), P Cyg ($-604\,\mathrm{km\ s^{-1}}$), and shell ($-50\,\mathrm{km\ s^{-1}}$) remain stationary from high to low state. The structure of the wind flow seem to be unchanged from high to low state, and only the emissivity of the gas at different velocities seems to change

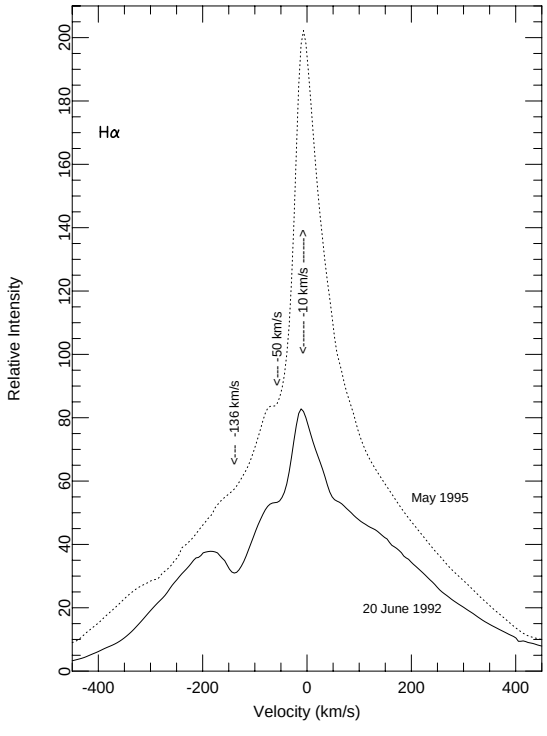

Fig. 8. Central portion of Hα line profile in high (dotted line) and low state (continuous line). The small velocity of the narrow component ($-10\,\mathrm{km\ s^{-1}}$) compared to $-40\,\mathrm{km\ s^{-1}}$ in other lines seems to be due to an absorption component centered at $-50\,\mathrm{km\ s^{-1}}$

velocity is measured at $I/I_c = 0.95$ (Eenens & Williams 1994; Crowter et al. 1997), $v_{\rm term} = -1350\,\mathrm{km\ s^{-1}}$ in low state. A narrow displaced component (NDC), resembling that frequently observed in the UV resonance lines of other hot stars, is seen at $rv = -1061\,\mathrm{km\ s^{-1}}$. On high state, emission fills up the high velocity regions of the P Cygni profile, except for the NDC, which becomes even more distinctive. This component seems to mark a region of critical transition in the wind flow. There is no clear sign that the wind flow properties are changing from high to low state. The high velocity structures in the He I λ10830 do not change in radial velocity. Variations in the profile of this line seem due to changes in the emissivity of the gas at different radial velocities, caused by an external source.

The absence of the narrow component in Balmer H lines seems to be due to the same mechanism that produces a shell component in the He I λ10830 line. In Figure 8, a faint absorption is seen at $-50\,\mathrm{km\ s^{-1}}$, the blue side of the Hα narrow component. This component makes the narrow component of Hα asymmetric and shifts its peak from the expected $-40\,\mathrm{km\ s^{-1}}$ to $-10\,\mathrm{km\ s^{-1}}$. The strength of this absorption component grows toward the head of the Balmer series, making the narrow component disappear at H 2-6, as seen in Fig. 9. The radial velocity of this absorption component is exactly the same as that of shell component in He I λ10830. The discovery of a true absorption, in place of the double-peaked profile referred to by previous authors, has important consequences for understanding the reddening and velocity field around η Car. The faintness of the narrow components in Balmer lines compared to Paschen series had been attributed to extinction effects. If that was the case, the broad components would suffer from extinction much more than the narrow components, as broad lines are formed in the inner stellar wind and narrow components in the surrounding gas (Davidson et al. 1997). The effect of extinction would cause Balmer lines to have profiles similar to those of the Paschen series, but with smaller *broad/narrow* flux ratio, contrary to the observations. The observed differences between Paschen and Balmer line series are more likely due to line opacity than extinction effects. The region that forms the absorption component at $rv = -50\,\mathrm{km\ s^{-1}}$

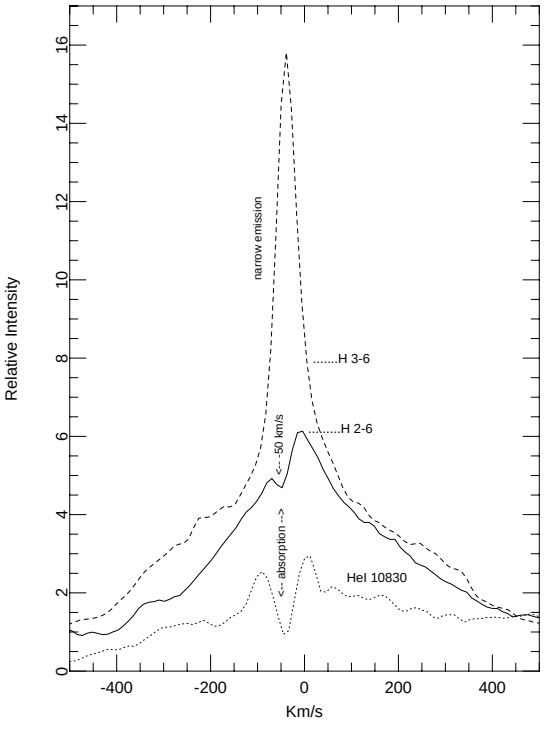

Fig. 9. Line profile of Paschen-γ compared with a Balmer-δ (same upper levels) in high state. H 2-6 (continuous line) shows a strong absorption component at $-50\,\mathrm{km\ s^{-1}}$ that shifts the peak of the narrow component to lower velocity than H 3-6 (dashed line). He I λ10830 (dotted line) on low state is displayed to reinforce the reality of this absorption feature

must be very dense in order to produce the remarkable absorption and probably has small spatial extent as the $fwhm$ is only 30 km s^{-1}, the smallest we measured in our spectra. Could it be produced by an equatorial disk?

The P Cygni components in H lines strengthen toward the upper members of each series, but with radial velocity increasing in the opposite sense. Radial velocities of the P Cygni components are higher on low state than in high state spectrum. The radial velocity curve as a function of wavelength flattens around $-500\,\mathrm{km\ s^{-1}}$ on low state and -470 km s^{-1} in high state. This is not, however, the terminal velocity of the wind, as the P Cygni component in the He I λ10830 line is more negative than in the other lines. A transition in the velocity regime occurs for quantum numbers $n = 5$ in the Balmer series and $n = 11$ in the Paschen series. There is a rapid increase in radial velocity for higher energy levels, which indicates that these features are formed in a region of fast acceleration. It is important to note that the broad components of H lines are shifted toward the blue when P Cygni components are stronger. If this was due to intrinsic variability in the wind, the strengthening of the P Cygni absorption would occur at the expense of the emission component, shifting the emission component toward longer wavelengths. Based on this fact, DCL attributed radial velocity variations in the barycenter of broad H line components to Doppler effect due to orbital motion in a binary system.

The Fe^+ lines have broad line components with $fwhm$ unchanged from high to low state. Radial velocity variations in the broad component is not evident in [Fe II] lines but is easily seen in many Fe II lines, especially from multiplets 27, 38, 42, 49, and 74. Some of these lines show permanent P Cygni components, which strengthen in low state. The P Cygni features in Fe II lines are more blueshifted in low than in high state, as also seen in H I, Si II, and N I lines (Fig. 5). We have not found the P Cygni components in [Fe II] lines reported by Aller & Dunham (1966). The Fe^+ broad line components show a discrepancy from the trend between $fwhm$ and ionization potential (Fig. 4). Both narrow and broad components of Fe^+ show a large scatter in $fwhm$, compared to other lines. The Fe II and [Fe II] lines show the similar $fwhm$ values, contrary to what was found in narrow line components by Hamann et al. (1994).

Si II λ6347 shows a very prominent P Cygni component for a brief time interval at the low state. This short-lived component (about 1 month) is a good tracer of the central phases of the spectroscopic event.

Na I $\lambda\lambda$5890−5 show seven absorption structures, superimposed on a broad emission. No substantial difference is seen in these components from high to low states. The changes seen in the blue extremity are likely due to the wings of He I λ5876 line. Besides the interstellar component and the strong P Cygni profile at $rv = -474\,\mathrm{km\ s^{-1}}$, the other five components at $rv = -103$, -210, -380, -440, and $-506\,\mathrm{km\ s^{-1}}$ are too faint to deserve special attention. The broad emission and the P Cygni components have velocity characteristics similar to that of other low excitation lines, indicating that they also are formed in the stellar wind.

Ca II H & K presents only P Cygni profiles at $rv = -470$ km s^{-1}, but emission components cannot be excluded, as these lines are blended at the red side.

7. Discussion and conclusions

We reviewed the identification of lines in the spectrum of η Car in the range 4040 Å to 10970 Å. Our spectra have higher resolution than previous published data, for the same wavelengths, allowing the deblending of line components for the majority of spectral features. Based on precise radial velocities and variability from high to low state, we identified several new lines of Fe II, [Fe II], [Fe III], and Ca II and rejected a number of previous identifications.

Line parameters in high and low excitation states are presented for the narrow line components separated from

the broad ones. We show that line strengths vary between these states in close relation to the excitation energy of the atomic transition. The higher the excitation level, the larger the fading of the line in low state. Broad components of several low excitation lines become stronger on low state, specially Fe II, [Fe II], and Ti II.

DCL suggested that η Car is an eccentric binary system in which the secondary component is hotter than the primary. Radial velocity changes of the broad line components of He I, H I, and Fe II between the high and low states are compatible with Doppler motion of the stellar wind, following the primary star along the orbit. The low state occurs at the time of periastron passage. The main X-ray properties of η Car like the temperature of the hard spectrum, the flux and column density variability are well accounted for by models of wind-wind collision in an eccentric binary system. Both the secondary star and the wind-wind collision zone produces high energy photons. In that model, the shocked zone becomes deeply enshrouded in the dense wind of the primary star at the periastron passage, screening the hard energy photons from reaching the outer layers of the stellar wind and the nebular region. The model fails just around the periastron passage, what indicates that something else than simple eclipses is playing an important role. It may be the a disk-like structure suggested by previous authors (see below).

The optical/NIR spectrum of η Car shows a mixture of high and low excitation lines, requiring more than one excitation source. Permitted lines indicate that the main ionization source is cooler than the star P Cygni (T = 18000 K, Lamers et al. 1996), as this star shows Si IV, Si III, [N III], and Fe III lines compared to Si II, [N II], and Fe II in η Car. Similar situation was found in the UV spectrum by Ebbets et al. (1997), who suggested a linear combination of spectral types B2 Ia and B8 Ia. In spite of the much denser wind in eta Car, Ebbets et al. (1997) showed that its spectrum is very similar to that of P Cygni. On the basis of our spectra we estimate the temperature of the primary star in the range $15\,000\,\mathrm{K} \leq T \leq 18\,000\,\mathrm{K}$. The spectral signatures of higher excitation comes from other(s) source(s) of energy in the system. Such temperature would place the primary star at the cooler side of the evolutionary track shown in Fig. 7 of DCL. A star at that position in the HR diagram is at the end of the H-burning and entering in the core He-burning stage. This implies that the LBV component will soon become a Wolf-Rayet star and the system will be similar to WR140, a WR+O colliding wind binary.

The huge variations observed in the strength of the high excitation lines are not accompanied by photometric variability at a significant level in the optical and UV energy ranges, indicating that the source of energetic photons must have a bolometric luminosity smaller than the primary one. The transition from high to low state spectrum occurs in time scale of 1 month. It is not clear if this behavior is due to an eclipse of the source of hard photons, as seen from the clouds emitting the narrow lines, or an intrinsic variation in the wind-wind colliding zone. In the case of eclipse, there must be some extended structure of high density gas around the primary star, in order to account for the long duration of the spectroscopic event that lasts for 2-8 months (depending on the energy level of the line). Both these mechanisms can explain why broad line components of He I lines fade when that of Fe II strengthens on low state. The lower excitation in the wind of the primary star, as seen from the Earth in low state, accounts for stronger P Cygni profiles and apparently unchanged velocities in the wind signatures. The exact mechanism that controls the excitation in η Car lines, however, must be studied in light of additional data.

The complete picture of the η Car system, however, is much more complicated than sketched above. The line profiles trace the existence of four main velocity structures:

- a high density, mildly excited stellar wind, accelerated up to $rv \sim -1350\,\mathrm{km\ s^{-1}}$, responsible for broad emission components of permitted lines and P Cygni profiles;
- a compact, slow moving gas layer ($rv \sim -50\,\mathrm{km\ s^{-1}}$), probably an equatorial disc, responsible for the shell absorption in He I λ10830 and Balmer lines;
- a nebular region with a mixing of high and low excitation narrow lines, in a narrow range of velocities ($fwhm \sim 60\,\mathrm{km\ s^{-1}}$, $rv \sim -40\,\mathrm{km\ s^{-1}}$), encompassing the Weigelt blobs around the Homunculus equator, responsible for the narrow line components;
- gas of intermediate velocity $rv \sim -350\,\mathrm{km\ s^{-1}}$) emitting high excitation lines, probably ejected from the wind-wind collision zone. Such a velocity field and the region of high density suggested above leads to a picture of the primary star with an equatorial disk and fast polar winds. Non-spherical winds have been suggested by previous authors: Viotti et al. (1989) Davidson et al. (1995), Davidson & Humphreys (1997) pointed out a connection between eta Car and B[e] stars (Zickgraf et al. 1986).

The bipolar flow is composed of two thin expanding shells of gas and dust, enclosing the central stars. Such geometry has been attributed to the initial conditions of the eruption that occurred in the last century. However, we've detected high speed gas ($rv = -1350\,\mathrm{km\ s^{-1}}$) that must be colliding against the internal walls of the Homunculus, causing an acceleratio by the continuous deposition of momentum from the stellar wind. In fact, the early η Car spectra (Walborn & Liller 1977) show velocities much lower than presently seen in the Homunculus. A B[e]-like star, with wind speeds increasing from the equator toward the polar regions, could have shaped a bipolar flow like the presently observed Homunculus.

Acknowledgements. AD thanks Peter Conti and JILA for the opportunity of spending a sabbatical year in Boulder and

to FAPESP and CNPq (Brazil) for financial support. AK's work was supported by the Deutsche Forschungsgemeinschaft (Wo 296/16-1,2). AK, OS, and BW want to thank all the FLASH/HEROS observers namely Th. Gäng, Th. Rivinius, C.A. Gummersbach, J. Peitz, J. Schweickhardt, J. Kovács, D. Schäfer, H. Mandel, Th. Szeifert, I. Jankovics, H. Lehmann, S. Štefl, D. Baade, U. Thiel, Th. Dumm, and W. Schmutz.

References

Abraham Z., Damineli A., 1997, IAUC 6768
Allen D.A., Jones T.J., Hyland A.R., 1985, ApJ 291, 280
Aller L.H., Dunham T. Jr., 1966, ApJ 146, 126
Altamore A., Maillard J.P., Viotti R., 1994, A&A 292, 208
Bandiera R., Focardi P., Altamore A., 1989, in IAU Coll. 113, Physics of Luminous Blue Variables, Davidson K., Moffat A.F.J., Lamers H.J.G.L.M. (eds.). Dordrecht: Kluwer, p. 279
Cannon A.J,, 1916, Harvard College Obs. Ann. 76, 36
Corcoran M.F., Ishibashi K., Swank J.H., et al., 1997, Nat 390, 587
Crowter P.A., Bohannan B., Pasquali A., 1997, in Boulder-Munich II: Properties of Hot Luminous Stars ASP Conf. Ser. 131, p. 38
Damineli A., 1995, Rev. Mex. Astron. Astrofis. (Serie de Conf.) 2, 41
Damineli A., 1996, ApJ 460, L49
Damineli A., Conti P.S. Lopes D.F., 1997, New Astron. 2, 107
Damineli A., Viotti R., Baratta G.B., Araujo F.X., 1993, A&A 268, 183
Davidson K., 1997, New Astron. 4, 387
Davidson K., Dufour R.J., Walborn N.R., Gull T.R., 1986, ApJ 305, 867
Davidson K., Ebbets D., Weigelt G., et al., 1995, AJ 109, 1784
Davidson K., Ebbets D., Johansson S., et al., 1997, AJ 113, 335
Davidson K., Humphreys R.M., 1997, Ann. Rev. A&A 35, 1
Duncan R.A., White S.M., Lim J., 1997, MNRAS 290, 680
Ebbets D., Morse J., Davidson K., Walborn N., 1997, in Luminous Blue Variables: Stars in Transition Lamers and Nota (eds.). ASP Conf. Ser. 120, p. 249
Ebbets D.C., Walborn N.R., Parker J.Wm., 1997 ApJ 489, L161
Eenens P.R.J. Williams P.M., 1994, MNRAS 269, 1082
Gaviola E., 1953, ApJ 118, 234
Hamann F., DePoy D.L., Johansson S., Elias J., 1994, ApJ 422, 626
Hoffleit D., 1933, Harvard Bull. 893, 11
Hillier D.J., Allen D.A., 1992, A&A 262, 153
Hofmann K-H., Weigelt G., 1988, A&A 203, L21
Jablonski F., Lopes D.F., Damineli A., 1998, IAUC 6849
Johansson S., Wallerstein G., Gilroy K.K., Joueizadeh A., 1995, A&A 300, 521
Johansson S., Hamann F.W., 1993, Phys. Scr. T47, 157
Kaufer A., Stahl O., Wolf B., et al., 1996, A&A 314, 599
Lamers H.J.G.L.M., Najarro F., Kudritzki R.P., et al., 1996 A&A 315, L225
Le Seuer A., 1870, Proc. R.S. 18, 245
Lopes D.F. Damineli A., 1997, IAUC 6790
Meaburn J., Gehring G., Walsh J.R., Palmer J.W., López J.A., et al., 1993, A&A 276, L21
McKenna F.C., Keenan F.P., Hambly N.C., et al., 1997, ApJS 109, 225
Rodgers A.W. Searle L., 1967, MNRAS 135, 99
Ruiz M.T., Melnick J. Ortiz P., 1984, ApJ 285, L19
Stevens I.R., Pittard J.M., Corcoran M.F., 1997, A&AS 191, 34.05
Thackeray A.D., 1953, MNRAS 113, 211
Thackeray A.D., 1967, MNRAS 135, 51
Thackeray A.D., 1969, M. N. R. A. South Africa 28, 37
Viotti R., 1968, Mem. Soc. Astr. Ital. 39, 105
Viotti R., 1995, Rev. Mex. Astron. Astrofis. (Serie de Conf.) 2, 1
Viotti R., Rossi L., Cassatela A., Altamore A., Baratta G.B., 1989, ApJS 71, 983
Walborn N.R. Lillier M.H., 1977, ApJ 211, 181
Whitelock P.A., Feast M.W., Carter B.S., Roberts G., Glass I.S., 1983, MNRAS 203, 385
Whitney C.A., 1952, Harvard Bull. 921, 8
Zanella R., Wolf B. Stahl O., 1984, A&A 137, 79
Zickgraf F.-J., Wolf B., Leitherer C., Appenzeller I., Stahl O., 1986, A&A 163, 119